tvst

Glaucoma

Visible Light Optical Coherence Tomography of Peripapillary Retinal Nerve Fiber Layer Reflectivity in Glaucoma

Weiye Song[1], Sui Zhang[2], Yumi Mun Kim[3], Natalie Sadlak[4], Marissa G. Fiorello[4], Manishi Desai[4], and Ji Yi[1,5,6]

[1] Department of Medicine, Boston University School of Medicine, Boston Medical Center, Boston, MA, USA
[2] Department of Epidemiology, School of Public Health, Johns Hopkins University, Baltimore, MD, USA
[3] Department of Philosophy & Neuroscience, Boston University, Boston, USA
[4] Department of Ophthalmology, Boston Medical Center, Boston, MA, USA
[5] Department of Ophthalmology, School of Medicine, Johns Hopkins University, Baltimore, MD, USA
[6] Department of Biomedical Engineering, Johns Hopkins University, Baltimore, USA

Correspondence: Ji Yi, Department of Opthalmology and Biomedical Engineering, Johns Hopkins University, 400 N Broadway, Baltimore, MD 21231, USA.
e-mail: jiyi@jhu.edu

Received: March 23, 2022
Accepted: August 19, 2022
Published: September 27, 2022

Keywords: visible light OCT; peripapillary nerve fiber layer reflectivity; glaucoma; VNOCT

Citation: Song W, Zhang S, Kim YM, Sadlak N, Fiorello MG, Desai M, Yi J. Visible light optical coherence tomography of peripapillary retinal nerve fiber layer reflectivity in glaucoma. Transl Vis Sci Technol. 2022;11(9):28, https://doi.org/10.1167/tvst.11.9.28

Purpose: To evaluate the clinical utility of visible light optical coherence tomography (VIS-OCT) and to test whether VIS-OCT reflectivity and spectroscopy of peripapillary retinal nerve fiber layer (pRNFL) are correlated with severity of glaucoma, compared with standard-of-care OCT thickness measurements.

Methods: In total 54 eyes (20 normal, 17 suspect/preperimetric glaucoma [GS/PPG], 17 perimetric glaucoma [PG]) were successfully imaged with complete datasets. All the eyes were scanned by a custom-designed dual-channel device that simultaneously acquired VIS-OCT and near-infrared OCT (NIR-OCT) images. A 5×5 mm^2 scan was taken of the pRNFL. The pRNFL reflectivity was calculated for both channels and the spectroscopic marker was quantified by pVN, defined as the ratio of VIS-OCT to NIR-OCT pRNFL reflectivity. The results were compared with ophthalmic examinations and Zeiss Cirrus OCT.

Results: VIS-OCT pRNFL reflectivity significantly, sequentially decreased from normal to GS/PPG to PG, as did NIR-OCT pRNFL reflectivity. The pVN had the same decreasing trend among three groups. Normal and GS/PPG eyes were significantly different in VIS-OCT pRNFL reflectivity ($P = 0.002$) and pVN ($P < 0.001$), but were not in NIR-OCT pRNFL reflectivity ($P = 0.14$), circumpapillary RNFL thickness ($P = 0.17$), or macular ganglion cell layer and inner plexiform layer thickness ($P = 0.07$) in a mixed linear regression model.

Conclusions: VIS-OCT pRNFL reflectivity and pVN better distinguished GS/PPG from normal eyes than Cirrus OCT thickness measurements.

Translational Relevance: VIS-OCT pRNFL reflectivity and pVN could be useful metrics in the early detection of glaucoma upon further longitudinal validation.

Introduction

Glaucoma is a leading cause of blindness worldwide, and the second leading cause of blindness in the United States.[1,2] Clinically, glaucomatous optic neuropathy is characterized by thinning in the peripapillary retinal nerve fiber layer (pRNFL) and a decrease in sensitivity in visual field testing.[3–5] Early detection of the structural damage to retinal ganglion cells (RGC) and their axons in the RNFL and within the optic nerve head is important for timely diagnosis, treatment and vision preservation. Optical coherence tomography (OCT)[6] has been the standard-of-care imaging modality to quantitatively measure the structural change of RNFL. The pRNFL and macular RGC thinning are used routinely in diagnosing glaucoma.[7–10] However, OCT thinning alone may be insufficient in early glaucoma detection. It is reported that the standard outside-normal-limit

analysis of global RNFL thinning yields a less than 35% accuracy in identifying progressing disease in glaucoma suspects.[11] Improving the detection sensitivity of early structural changes in glaucoma would be beneficial.

Laboratory studies have shown that changes in the RGC axon cytoskeleton can be detected by RNFL spectroscopic contrast and that these features may represent nanoscale change in microtubules before axon loss and consequent RNFL thinning.[12–14] Visible light OCT (VIS-OCT) is a recent development that uses shorter wavelengths than the near-infrared (NIR) wavelengths used in standard OCT devices.[15–17] Initial data show that the spectral contrast between VIS-OCT and NIR-OCT may reveal information from which nanoscale structural features can be quantitatively inferred[18–21] at a scale beyond the image resolution by standard OCT images.[22,23] This approach, when applied to clinical reflectance spectroscopy, may provide better sensitivity on RNFL alterations than current OCT thickness measurements in early glaucoma.

We recently developed a dual-channel clinical OCT device that can simultaneously acquire VIS-OCT and NIR-OCT using a robust fiber optics design.[18] A novel metric (i.e., pVN) was derived from reflectance spectroscopy, by the intensity ratio between VIS-OCT and NIR-OCT images. We identified changes in RNFL of ocular hypertensive mice using pVN.[24] The goal of the present study was to compare our two-channel VIS-OCT metrics with standard OCT outcomes among normal, glaucoma suspect/preperimetric (GS/PPG), and perimetric glaucoma patients in a cross-sectional study.

Methods

Study Design and Subject

This cross-sectional study was conducted at Boston Medical Center eye clinics, from March 2019 to January 2020, whose Institutional Review Board reviewed and approved the study. The study was compliant with the Health Insurance Portability and Accountability Act and adhered to the tenets of the Declaration of Helsinki. Written informed consent was obtained from all subjects before participation. Inclusion criteria were patients ages 40 years or more and a best-corrected visual acuity of better than 20/40. Exclusion criteria included previous intraocular surgery other than uncomplicated cataract surgery, angle-closure glaucoma, and a history of diabetic retinopathy, vascular occlusion, macular degeneration, macular edema, hereditary retinal degeneration, uveitis, and other retinal conditions. Because visible light has shorter wavelength than NIR and is more sensitive to cataract and lens changes, eyes with a best-corrected vision acuity of worse than 20/40 were excluded to decrease this confounding factor for lens in this pilot study. Cataracts were evaluated using the Lens Opacification System II based on color and opalescence.[25] The system uses a 4-point grading system with increasing number consistent with increasing maturity. Severe cataracts graded more than 2+ were excluded.

Study subjects were recruited during their standard-of-care visit. Normal subjects were recruited from optometry clinics. Normal eyes were defined as having a normal appearance of the optic nerve and by stereoscopic optic disc photograph assessment at the point of care (subjective assessment of vertical cup-disc ratio), as well as having no history of an intraocular pressure of greater than 22 mm Hg. GS/PPG eyes were defined as having an optic disc appearance judged to potentially represent glaucomatous optic neuropathy on stereoscopic optic nerve examination, but having normal visual field test by Zeiss 24-2 threshold test: a glaucoma hemifield test either within normal range or borderline, and a pattern standard deviation index of less than 5%. Perimetric glaucomatous (PG) eyes were defined as having an optic disc appearance judged to be compatible with glaucoma and reliable, abnormal visual fields: a glaucoma hemifield test result outside normal limits or a pattern standard deviation index of less than 0.05%. Both eyes were imaged if eligible.

All subjects underwent an ophthalmic examination including tonometry, stereoscopic optic disc assessment, and clinical OCT imaging (Cirrus, Zeiss, Jena, Germany). The RNFL thickness at the peripapillary and macular regions, average cup-disc ratio, and vertical cup-disc ratio were quantitatively derived from standard OCT. Humphrey central 24-2 threshold tests were taken for GS/PPG and PG subjects, and the mean deviation (MD) and pattern standard deviation were recorded. After the clinical and ophthalmic examinations, dual-channel VIS-OCT was performed subsequently, and RNFL reflectivity metrics were quantified. The patients were imaged by trained technicians.

Research Dual-Channel VIS-OCT Device

A custom-built dual-channel VIS-OCT device was used to acquire optic disc cubes from every subject (Fig. 1a). Each scanning cube had 256 B-scan frames, and each B-scan had 512 A-lines. Each scan covered an approximately 5 × 5 mm^2 area. Further technical details of the device were described in our previ-

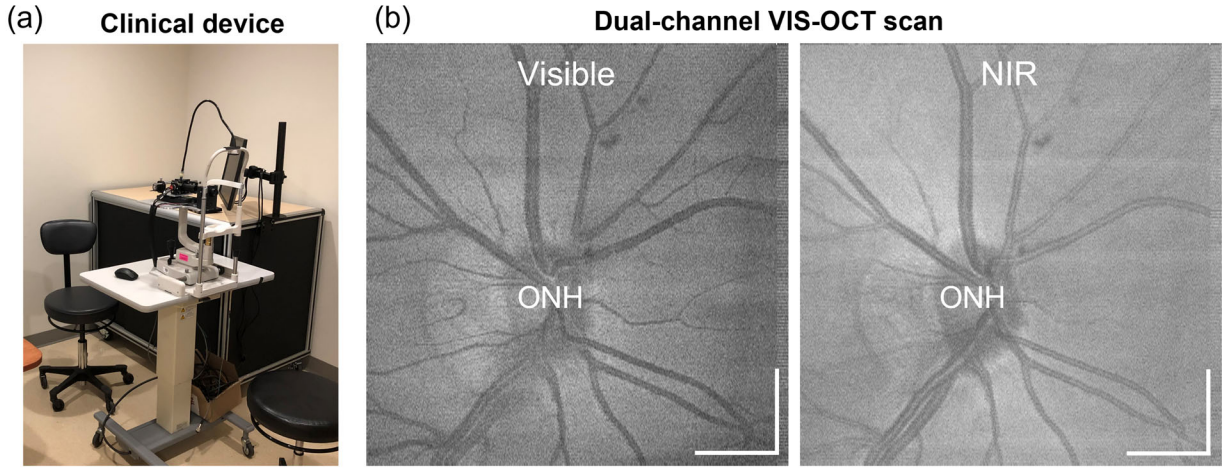

Figure 1. (a) Photograph of dual-channel VIS-OCT device. (b) En face projections of the optic disc scan in the visible and NIR channels, respectively. Bar, 1 mm.

ous publications.[18] The visible light channel used a supercontinuum source (SuperK Extreme, EXU-OCT-6, NKT, Brondby, Denmark), and the NIR channel used a superluminescent laser diode (SLD-CS-371-HP3-SM-840-I, Superlum, Moscow, Russia). A custom-built spectrometer was used for VIS-OCT,[26] and a commercial one (CobraS 800, Wasatch Photonics, Morrissville, NC) was used for NIR-OCT. The visible channel used 545 to 580 nm light as the light source, and the NIR channel used wavelengths at 800 to 880 nm, defined by their respective spectrometers. The laser powers on the pupil were 0.25 mW and 0.9 mW for VIS- and NIR-OCT. The cumulative visible and NIR power is well within the laser safety level (see Supplementary Appendix A for detailed calculation).

We installed an electric tunable lens to accommodate the spherical refractive error. The fellow eye was used for fixation. The NIR channel was used for the initial alignment, then the visible light channel was turned on for fine tuning and simultaneous dual-channel imaging. The acquisition time was 2.6 s at 50 kHz A-line speed. Image examples are shown in Figure 1b.

RNFL Reflectivity Metrics and Processing

All the image processing was based on the linear scale of OCT images. The pRNFL reflectivity metrics included VIS pRNFL-R (*p*eripapillary *RNFL r*eflectivity in VIS-OCT), NIR pRNFL-R (*p*eripapillary *RNFL r*eflectivity in NIR-OCT), and pVN (ratio of *V*IS pRNFL-R and *N*IR pRNFL-R). The processing for each parameter is described elsewhere in this article.

The manual segmentation was performed on NIR-OCT images to label the retinal surface, the bottom edge of RNFL, and retinal pigment epithelium (RPE). Dense points were first marked on the boundaries in ImageJ, and linear interpolations were performed within B-scans and subsequently along the slow direction. After the segmentation on NIR-OCT images, we registered VIS-OCT and NIR-OCT images and applied the same segmentation to both channels. The RNFL and sub-RNFL layers were isolated as illustrated in Figure 2. The noise background, I_{noise}, was first obtained by averaging the signal within 30 to 40 µm above the retina surface and then subtracted from the image cube. To quantitate RNFL reflectivity, the following processing was performed. En face regions of interest (ROIs) were manually selected to avoid the major vessels. The same en face ROI selections were applied to both channels. OCT signals within RNFL were summed, normalized by the thickness per A-line, and then averaged within areas in all ROIs.

$$I_{RNFL} = \frac{1}{A}\sum_{x=1}^{n}\sum_{y=1}^{m}\left[\frac{1}{T(x,y)}\sum_{z=1}^{i} I(x,y,z)\right], \quad (x,y) \in ROIs \tag{1}$$

where $I(x,y,z)$ is the cubic OCT signal and I_{RNFL} is the RNFL signal. A is the total en face area of the selected ROIs, and $T(x,y)$ is the RNFL thickness at each A-line. To account for the signal variation between eyes, we used the same method to calculate $I_{sub\text{-}RNFL}$ within the sub-RNFL layer and quantitate RNFL reflectivity by,

$$pRNFL - R = \frac{I_{RNFL}}{I_{sub-RNFL}}. \tag{2}$$

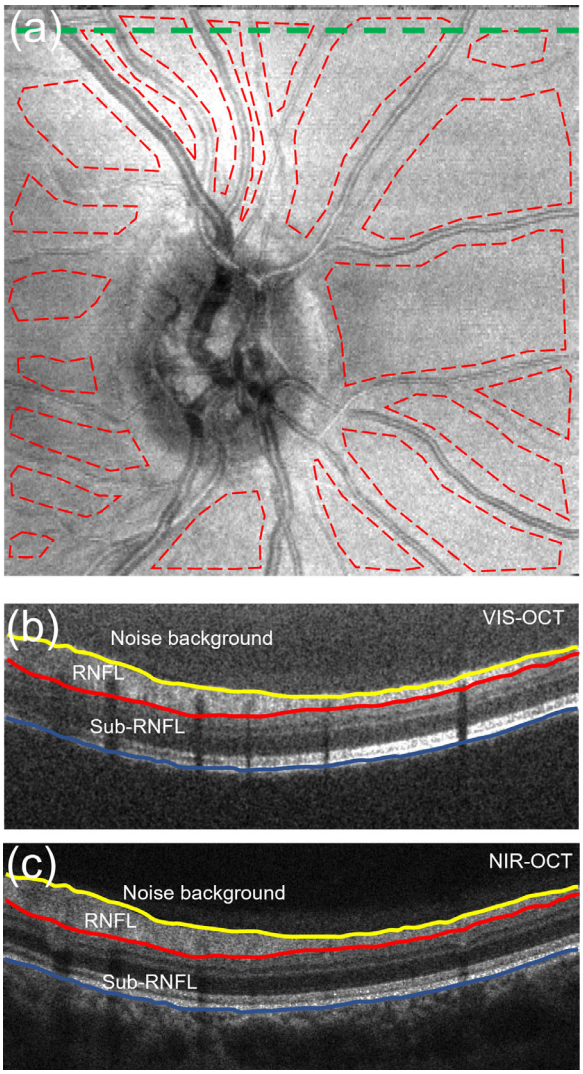

Figure 2. (a) Illustration of the *en face* ROIs selection. Red dashed line outlines the ROIs. (b, c) Segmentation for RNFL and sub-RNFL layer in VIS-OCT and NIR-OCT, respectively. B-scans in both channels were registered so that the same segmentation could be applied. B-scans were taken from the green dashed line in (a).

We then termed pRNFL reflectivity by VIS pRNFL-R and NIR pRNFL-R in the visible and NIR channels, respectively. The spectroscopic reflectivity contrast was further quantified by pVN defined as,

$$pVN = \frac{VIS\ pRNFL - R}{NIR\ pRNFL - R}. \quad (3)$$

Statistical Analyses

The χ^2 test or one-way analysis of variance were used to test the significance among three groups for categorical or continuous variables in the demographic information and ophthalmic examinations. For variables by Zeiss OCT and dual-channel VIS-OCT, Spearman rank tests or two-sample *t* tests were used to evaluate the association with the three groups of subjects. Receiver operating characteristic analysis was used to evaluate detection accuracy based on univariate logistic prediction. Mixed linear regression models were used to account for intersubject variations, considering some subjects had both eyes imaged. A negative logarithmic transformation was applied to the MD to improve the normalcy distribution in the mixed linear regression. When the MD was greater than 0, the MD was set to be the maximum negative MD value in this study. The adjusted average and the 95% confidence interval were calculated by a mixed linear model to evaluate the impact of severity and cataract to individual variables. All statistical analysis was performed using SAS 9.4 (SAS Institute, Cary, NC).

Results

Characteristics of Study Subjects

The study included 36 subjects (11 normal, 12 GS/PPG, 13 PG), and in total 54 eyes (20 normal, 17 GS/PPG, 17 PG) were successfully imaged with completed datasets. Among the other 18 eyes, two were excluded because of severe cataracts. Eyes with failed fixation were excluded. Examples of pRNFL reflectivity, Zeiss OCT, and 24-2 visual field tests are shown in Figure 3. There is no statistical difference among groups on age, gender, race, and ethnicity distributions (Table 1). By examining the demographic and ocular characteristics of study eyes (Table 2), there was a moderate increasing percentage of cataracts from normal, to GS/PPG, to PG eyes. The cup-disc ratio and vertical cup-disc ratio were significantly higher in GS/PPG and PG eyes than normal eyes. Zeiss Cirrus OCT thickness parameters (cpRNFL, GCL+IPL) were monotonically related among three groups, as well as VIS pRNFL-R, NIR pRNFL-R, and pVN.

Clinical Performance for Dual-Channel VIS-OCT Markers

Both VIS pRNFL-R and NIR pRNFL-R decreased from normal to GS/PPG to PG groups (Figs. 4a, 4b). The spectroscopic marker pVN also decreased, suggesting that the change of RNFL reflectivity is more dominant in visible channel than NIR (Fig. 4c). Between GS/PPG and PG eyes, both VIS pRNFL-R and NIR pRNFL-R were significant.

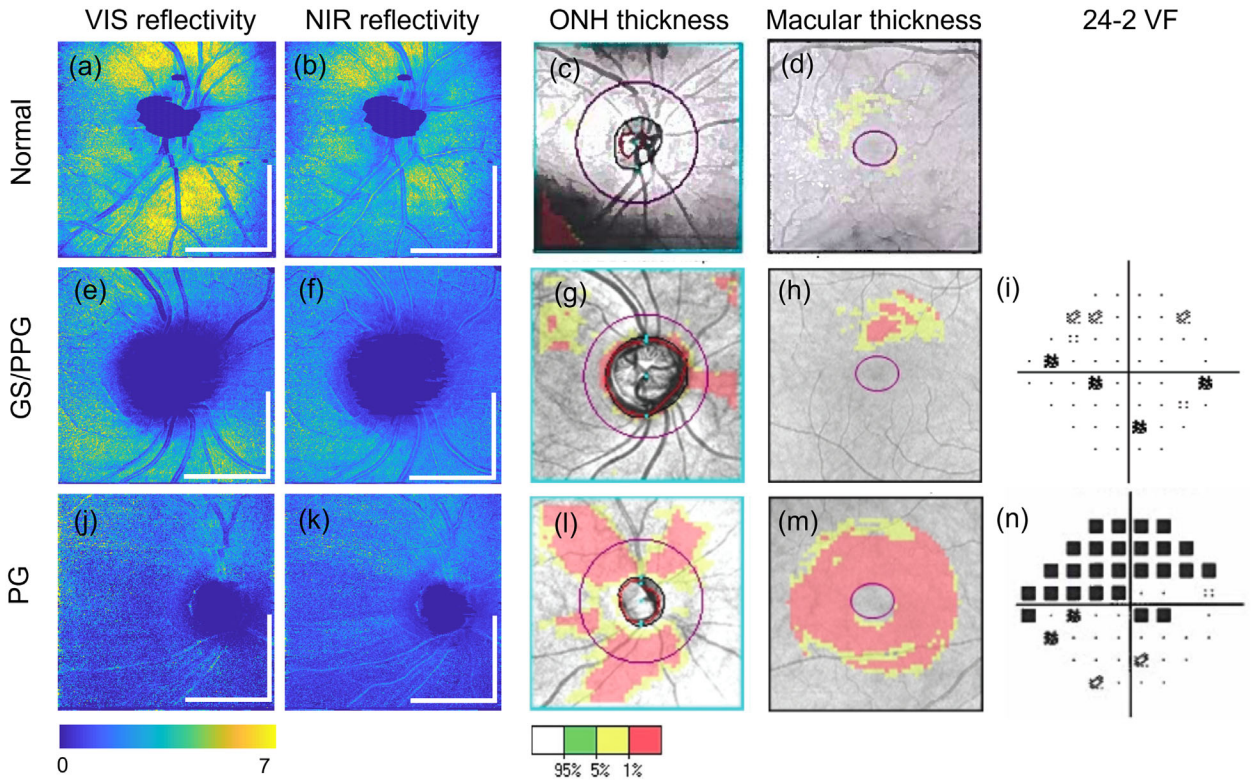

Figure 3. Comparison of pRNFL reflectivity in visible and NIR channel, ONH, and macular OCT scans, and visual field test in three examples, one from each group. (a–f) En face mapping of VIS-pRNFL-R and NIR-pRNFL-R from dual-channel OCT measurements. (g–l) ONH and macular cube scan by Zeiss Cirrus OCT with the thickness abnormality. (m, n) A 24-2 pattern deviation map. Bar, 2 mm.

Table 1. Demographic Information of Study Subjects

	Normal	GS/PPG	PG	*P* Value
No. of subjects	11	12	13	
No. subjects for both eyes imaged	9	5	4	
Age (y), mean ± SD	61.1 ± 12.9	62.8 ± 10.7	61.9 ± 11.1	0.93[a]
Gender (female/male)	4/7	5/7	4/9	0.76
Race (AA/White/others)	5/3/3	7/4/1	7/4/2	0.84
Ethnicity (Hispanic/non-Hispanic)	3/6[b]	1/11	1/12	0.13

AA, African American.
Categorical variables were compared among groups by the χ^2 test.
[a]One-way analysis of variance test was used.
[b]Unknown for two subjects.

In comparison with OCT thickness measurements, pVN and VIS pRNFL-R had higher significance in separating normal and GS/PPG eyes. Neither GCL+IPL nor cpRNFL was significantly different between normal and GS/PPG eyes (Figs. 4d–4g). We further examined superior and inferior cpRNFL thicknesses and found inferior cpRNFL better separated PG from other two groups. No significant difference was found in either quadrant of cpRNFL thickness between normal and GC/PPG eyes. A similar analysis was performed on reflectivity and pVN in superior and inferior quadrants (see Appendix B in the Supplementary Materials). Inferior VIS pRNFL-R and pVN were more significant in differentiating normal and GS/PPG eyes than superior, whereas superior was more significant in separating GS/PPG and PG eyes. Receiver operating characteristic analysis also showed that pVN and VIS pRNFL-R had the higher area under the curve

Table 2. Demographic and Ocular Characteristics of Study Eyes

	Normal	N>GS/PPG	N>PG	N>*P* Value
No. of eyes	20	17	17	
Age (y), mean ± SD	60.2 ± 12.7	62.1 ± 9.8	61.9 ± 10.6	0.86[a]
Side (OS/OD)	10/10	9/8	9/8	0.98[b]
Gender ratio (female/male)	7/13	9/8	5/12	0.34[b]
Ophthalmic examination				
Cataract (yes/no)	11/9	11/6	15/2	0.09[b]
Pseudophakic lens (yes/no)	5/15	4/13	2/15	0.33[b]
IOP (mm Hg), mean ± SD	15.3 ± 2.0	15.4 ± 3.7	14.1 ± 3.7	0.52[a]
Visual field test				
24-2 MD (dB), mean ± SD	–	−0.6 ± 1.2	−7.0 ± 5.4	**0.0002**[c]
24-2 PSD (dB), mean ± SD	–	1.8 ± 0.4	7.1 ± 5.0	**0.0004**[c]
Zeiss OCT				
GCL+IPL (μm), mean ± SD	77.8 ± 8.5	72.6 ± 8.6	64.4 ± 11.3	**0.0006**[d]
cpRNFL (μm), mean ± SD	89.8 ± 9.4	84.4 ± 14.3	67.9 ± 14.0	**<0.0001**[d]
Averaged CDR, mean ± SD	0.5 ± 0.2	0.7 ± 0.1	0.7 ± 0.1	**<0.0001**[d]
VCDR, mean ± SD	0.5 ± 0.2	0.7 ± 0.1	0.7 ± 0.1	**<0.0001**[d]
Dual-channel VIS-OCT				
VIS pRNFL-R, mean ± SD	3.4 ± 0.9	2.5 ± 0.7	2.0 ± 0.6	**<0.0001**[d]
NIR pRNFL-R, mean ± SD	2.5 ± 0.5	2.2 ± 0.5	1.9 ± 0.4	**0.0003**[d]
pVN, mean ± SD	1.4 ± 0.2	1.1 ± 0.2	1.0 ± 0.1	**<0.0001**[d]

CDR, cup-disc ratio; cpRNFL, circumpapillary retinal nerve fiber layer thickness; IOP, intraocular pressure; GCL+IPL, ganglion cell layer and inner plexiform layer thickness in macular scan; MD, mean deviation; PSD, pattern standard deviation; VCDR, vertical cup-disc ratio.

Dual-channel VIS-OCT markers are averaged values from all ROIs per eye. Bold indicates $P < 0.05$.

[a]One-way analysis of variance was used.

[b]The χ^2 test was used for categorical variables.

[c]Two sample *t* test was used.

[d]Spearman rank tests were used to evaluate the changes of variables among three groups.

in comparison with GCL+IPL in separating GS/PPG from normal eyes (Table 3). At the same time, VIS-OCT markers had lower area under the curve values than cpRNFL in differentiating GS/PPG and PG eyes.

Correlation Between Dual-Channel VIS-OCT and Standard Zeiss OCT

Spearman correlation tests showed that all markers from dual-channel VIS-OCT had excellent correlation with cpRNFL (Table 4). VIS pRNFL-R and pVN were highly correlated with GCL+IPL, as well as MD. Descriptive population statistics suggested that VIS-pRNFL-R and pVN had better association with visual field and Cirrus OCT measurements than NIR-pRNFL-R. To further test VIS-pRNFL-R and pVN's correlation with glaucoma severity (measured by cpRNFL and MD), a mixed linear regression model was used to account for individual variation because some of subjects had both eyes imaged. In the model where pVN was the dependent variable, and cpRNFL and MD were independent variables, both cpRNFL ($P = 0.003$) and MD ($P = 0.033$) were significant correlated with pVN. If we consider only within glaucomatous eyes, both cpRNFL ($P < 0.001$) and MD ($P = 0.006$) remained significant when VIS pRNFL-R was the dependent variable. VIS pRNFL-R and pVN were consistently correlated with cpRNFL in different tests.

Cataract Impact to Imaging Markers

We found that the GS/PPG and PG groups had more eyes with cataracts than the ones in normal group (Table 2), which could confound imaging markers. Mixed linear model regression was used to take glaucoma severity (as groups) and presence of cataracts as independent variables, where different imaging markers were dependent variables (Table 5).

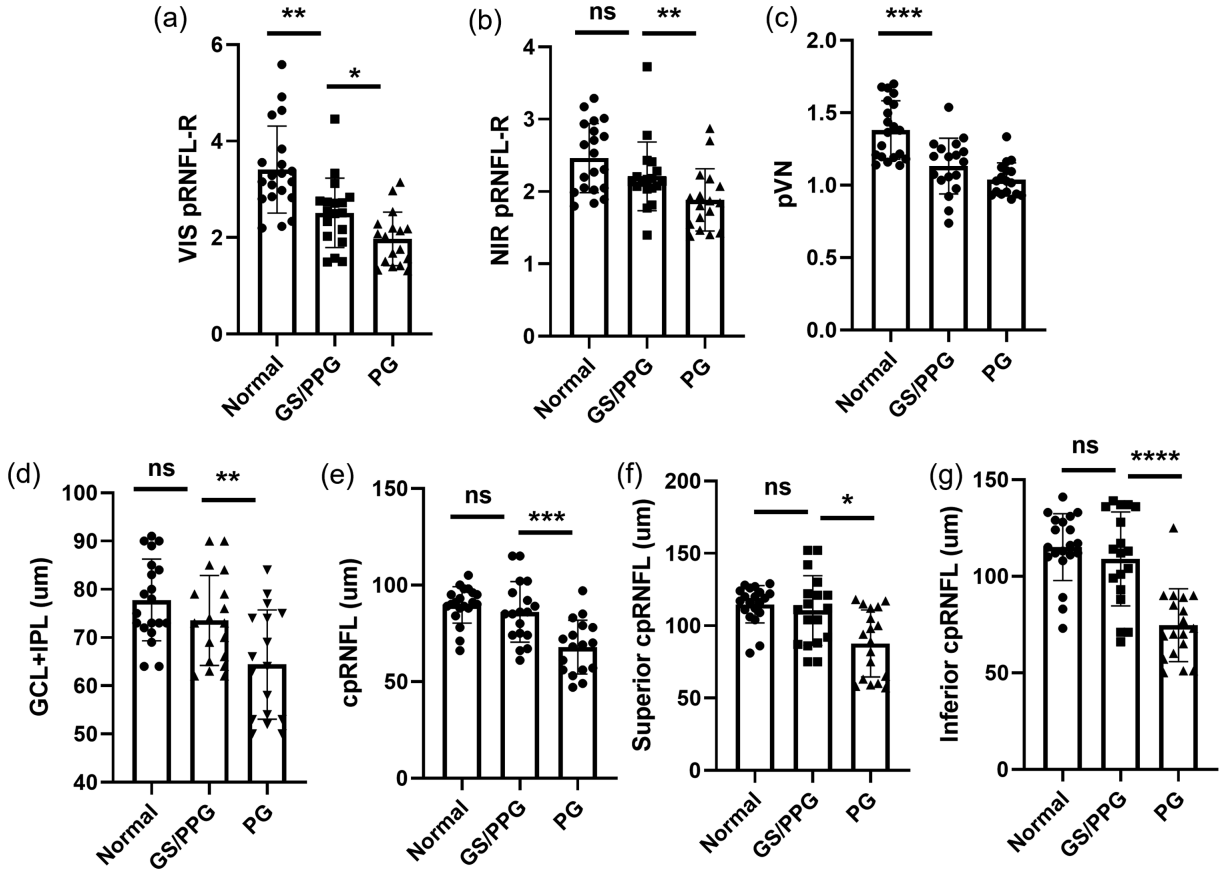

Figure 4. (a–c) The pRNFL reflectivity in VIS- and NIR-OCT channels, and pVN ratio in three groups of subjects. (d–g) Zeiss OCT thickness in three groups of subjects. Two sample *t* test was used to test significance within two groups. *$P < 0.05$, **$P < 0.01$, ***$P < 0.001$. The error bar is the SD.

Table 3. Area Under the Curve by Receiver Operating Characteristic Analysis

	Normal vs. GS/PPG	GS/PPG vs. PG	Normal vs. GS/PPG + PG
VIS pRNFL-R, (95% CI)	0.824 (0.684–0.963)	0.723 (0.547–0.900)	0.882 (0.793–0.972)
NIR pRNFL-R, (95% CI)	0.638 (0.449–0.827)	0.723 (0.540–0.907)	0.731 (0.590–0.872)
pVN, (95% CI)	0.788 (0.642–0.935)	0.671 (0.475–0.867)	0.872 (0.781–0.963)
GCL+IPL, (95% CI)	0.663 (0.484–0.842)	0.690 (0.507–0.873)	0.730 (0.596–0.864)
cpRNFL, (95% CI)	0.650 (0.455–0.845)	0.801 (0.651–0.951)	0.773 (0.642–0.903)

CI, confidence interval.
Receiver operating characteristic analysis is based on univariate logistic prediction.

VIS pRNFL-R ($P = 0.002$) and pVN ($P < 0.001$) remained significant in separating normal and GS/PPG eyes, and VIS pRNFL-R ($P = 0.043$) and NIR pRNFL-R ($P = 0.017$) were still significant in separating GS/PPG and PG eyes, with the presence of cataract. The pVN had higher significance in separating normal and GS/PPG eyes than VIS pRNFL-R. Neither GCL+IPL nor cpRNFL significantly differentiated between normal and GS/PPG eyes. Figure 5 further illustrates the adjusted averages (95% confidence interval) for eyes in the three groups with and without cataract. The *P*-interaction suggested that cataract had no significant impact on the association between dual-channel VIS-OCT markers, Cirrus OCT thickness, and glaucoma severity. The decreasing trends for all dual-channel VIS-OCT markers with increasing severity were consistent with and without cataract.

Table 4. Correlation Among Dual-Channel VIS-OCT, Zeiss OCT, and Visual Field Measurements

	VIS pRNFL-R	NIR pRNFL-R	pVN	GCL+IPL	cpRNFL
NIR pRNFL-R	**0.83 (<0.001)**				
pVN	**0.82 (<0.001)**	**0.43 (0.001)**			
GCL+IPL	**0.61 (0.011)**	0.24 (0.077)	**0.49 (<0.001)**		
cpRNFL	**0.35 (<0.001)**	**0.45 (0.001)**	**0.73 (<0.001)**	**0.76 (<0.001)**	
MD[a]	**0.45 (0.009)**	0.32 (0.073)	**0.46 (0.006)**	**0.42 (0.011)**	**0.41 (0.015)**

Spearman correlation was used to test the significance. *P* Values are given in brackets. Bold indicates $P < 0.05$.
[a]Calculation is done within GS/PPG and PG.

Table 5. Adjusted Average Values by Mixed Linear Model in the Three Groups

	Normal	GS/PPG	PG	P1: Normal vs. GS/PPG	P2: GS/PPG vs. PG
VIS pRNFL-R, (95% CI)	3.42 (0.35)	2.58 (0.37)	2.16 (0.39)	N>G: **0.002**	G>P: **0.043**
NIR pRNFL-R, (95% CI)	2.46 (0.24)	2.27 (0.24)	1.96 (0.25)	N>G: 0.137	G>P: **0.017**
pVN, (95% CI)	1.39 (0.08)	1.14 (0.08)	1.08 (0.10)	N>G: **<.001**	G>P: 0.15
GCL+IPL (μm),	78.13 (2.62)	72.76 (2.47)	64.22 (2.55)	N>G: 0.073	G>P: <**.001**
cpRNFL (μm),	90.65 (3.29)	86.34 (3.12)	69.92 (3.21)	N>G: 0.173	G>P: <**.001**

CI, confidence interval.
Adjusted averages were estimated by linear mixed model regression, considering the presence of cataract and the potential correlation between two eyes from a same subject. P1, P2 was assessed using post hoc Tukey's honest significant difference test. Bold indicates $P < 0.05$.

Discussion

Our pilot study demonstrated the feasibility of VIS-OCT in peripapillary imaging in clinical subjects. The dual-channel device provided simultaneous imaging with VIS-OCT and NIR-OCT, as well as reflectance spectroscopy by contrasting two channels. The dual-channel design allows for ease of alignment using NIR light without excessive exposure of visible light before acquisition. We found a progressive decrease in both pRNFL reflectivity in VIS-OCT and NIR-OCT with increasing severity of glaucoma, and the same trend for pVN, indicating that reflectivity decreases more in the visible channel. Importantly, the VIS pRNFL reflectivity and pVN are more sensitive in separating GS/PPG from normal eyes than pRNFL and GCL+IPL thinning. We also showed that pVN has better significance than visible pRNFL reflectivity in differentiating GS/PPG and normal eyes (Table 5), presumably owing to the improved robustness from normalizing VIS-OCT by NIR-OCT. Another markable difference between VIS-OCT and NIR OCT is that VIS-OCT has limited penetration beyond the RPE into the choroid. This is due to the stronger attenuation of visible light by melanin than NIR light. Although this factor may limit VIS-OCT's use for imaging deep choroid beyond retina, the whole retina can still be well-resolved.

The biophysical origin for the RNFL reflectance and spectroscopy has been extensively studied by Knighton and Huang[27] through a multispectral imaging microreflectometer. Cytoskeletons in the axon of RGCs attribute to the reflectance signal, particularly microtubules.[12] Using an ocular hypertension glaucoma rat model, it was found that all cytoskeleton components were distorted and damaged, leading to a decrease in the RNFL reflectance signal.[13] This decrease preceded RNFL thinning.[14] A light scattering model elucidated that the loss of microtubules contributed to the spectroscopic change in RNFL, causing nonuniform changes in RNFL reflectance across wavelengths.[13] The RNFL reflectance was decreased in glaucomatous retinas more in visible than in NIR wavelengths. This finding is consistent with our data that pRNFL reflectivity in both channels exhibited declining trends with glaucoma severity, as did pVN. The decrease of pVN is also consistent with our in vivo study with an ocular hypertension mouse model using dual channel VIS-OCT.[24] It is important to note that the spectroscopic change is sensitive to loss of microtubules in the length scale of tens of

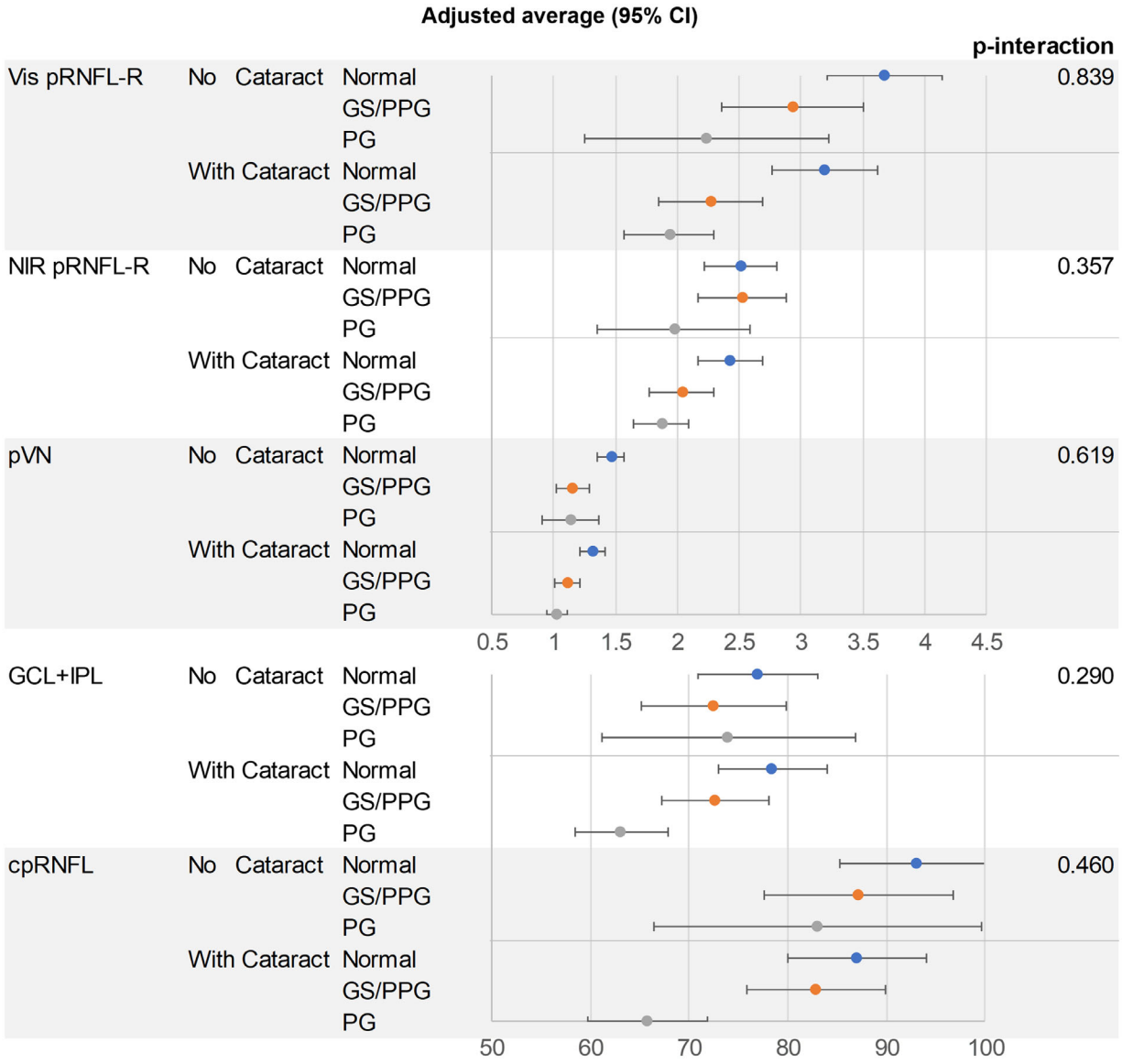

Figure 5. Adjusted average by mixed linear model regression, considering the potential correlation between two eyes from a same subject.

nanometer, beyond the resolution capability of any in vivo ophthalmic imaging modalities. The superb sensitivity of using spectroscopy is indeed well-documented in the biophotonics field,[22,23,28,29] supporting that RNFL reflectance spectroscopy could be an early detection method for glaucoma.

The existing clinical studies using RNFL reflectance in glaucoma are in general in line with our findings. A cross-sectional study showed that the decrease in RNFL reflectivity is associated with glaucoma, and could better distinguish preperimetric glaucoma from normal eyes.[30] However, the study used the summed intensity within RNFL and could be confounded by the RNFL thickness. Another longitudinal study reported a decrease in the RNFL reflectance may predict functional deterioration of glaucoma progression when combined with the rate of RNFL thinning.[31] Importantly, the data processing methods in these two studies were based on images taken from standard OCT devices. They likely used conventional OCT image intensity on a logarithmic scale, which could blunt the contrast and limit the sensitivity. In contrast, we used the linear scale images for calculating the reflectance signal. We performed a normalization to pRNFL thickness (Equation 1) and the sub-RNFL tissue intensity (Equation 2), and calculated the pVN by the ratio between two channels (Equation 3). Normalization to pRNFL thickness removes the confounder of RNFL thinning. Normalizing RNFL reflectance by sub-RNFL signals removes other

systemic wavelength-dependent attenuation, since light attenuation through anterior chamber, lens, and vitreous may be different in VIS-OCT and NIR OCT. These processing steps may contribute to better sensitivity of VIS-OCT RNFL reflectivity in separating GS/PPG from normal eyes.

We note that sub-RNFL included the outer retina and RPE. The assumption is that the pathological changes in glaucoma are primarily in RGCs, their dendrites (IPL) and axons (RNFL), which are independent of the outer retina and RPE. We calculated an alternative pVN without the I_{sub_RNFL} normalization in Supplementary Appendix C, where pVN = VIS I_{RNFL}/NIR I_{RNFL}; and found that the pVN still decreased from normal, to GS/PPG and PG eyes. However, the variations in each group are significantly greater , and the difference between GS/PPG and PG is insignificant. This comparison suggests that, although there can be variations in the I_{sub_RNFL} among eyes, the benefits of the normalization in Equation 2 to remove image quality variation and the systemic wavelength-dependence outweigh the caveat. The more comprehensive analysis of the optimal normalization and image processing would benefit from a larger scale study in the future.

Although the visible RNFL reflectivity and pVN have the best separations between normal and GS/PPG eyes than RNFL thinning, they may reach a floor effect[32,33] more quickly (i.e., less significant difference between GS/PPG and perimetric glaucoma eyes) than RNFL thickness. This behavior implies that both metrics are earlier events than thinning, presumably owing to the nanoscale sensitivity.

There are several limitations in our study. First, patient number in this pilot study is limited. Further validation will benefit from a larger number of subjects. Second, study this is cross-sectional, with no indication of whether VIS-OCT pRNFL reflectance and pVN can be predictive of progression. Third, patients with severe cataract were excluded, because of the unquantifiable VIS-OCT image quality. Owing to the laser power limitation and shorter wavelength, VIS-OCT is more susceptible to scattering attenuation from cataract. Fourth, the current layer segmentation and the selection of ROIs were performed manually in this study for accuracy. Automatic software will be developed to rapidly perform the processing. Finally, to facilitate the recruitment for normal subject, we recruited the subjects from optometry clinics and did not include visual field testing because it would take longer time for subject to participate in addition to Cirrus OCT and VIS-OCT. We will include visual field testing for all eyes in our future studies to have a complete dataset. Nevertheless, stereoscopic and Cirrus OCT examinations confirmed there is no glaucoma-appearing signs within normal eyes.

Future work includes continuing to improve the VIS-OCT device by having better light source stability, detection sensitivity, optimizing and standardizing the imaging protocol, and streamlining the data processing. One major practical challenge using VIS-OCT in clinics is the eye fixation and focusing. Although we used NIR-OCT for initial focus before switching on VIS-OCT, the fine tuning would typically still take 2 to 5 seconds, which can cause eye fixation to drift. This factor was the primary reason for the failed cases in the beginning of the study. The imaging success rate dramatically improved at later stage of the study as we gained more experiences. The imaging yield can be further improved by better confocal optics between two channels, and by implementing autofocusing and eye tracking. Beyond the scattering spectroscopy exploited here, VIS-OCT enables high resolution[34,35] and accurate microvascular retinal oximetry.[26,36–38] By using the technology offered by VIS-OCT, we can continue to enhance our ability to understand the sequence of physiologic changes in glaucoma in addition to improving our ability to detect abnormalities earlier. This technology also may have applications in other retinal pathologies.

Acknowledgments

The authors thank Harry Quigley, Pradeep Ramulu, and Thomas V. Johnston for valuable discussion and comments for this article.

Supported by BrightFocus foundation (G2017077), NEI/NINDS R01NS108464, NEI R21029412, R01EY032163, and NCI R01CA232015.

Disclosure: **W. Song**, None; **S. Zhang**, None; **Y.M. Kim**, None; **N. Sadlak**, None; **M.G. Fiorello**, None; **M. Desai**, None; **J. Yi**, None

References

1. Quigley HA, Broman AT. The number of people with glaucoma worldwide in 2010 and 2020. *Br J Ophthalmol*. 2006;90(3):262–267, doi:10.1136/bjo.2005.081224.
2. Friedman DS, Wolfs RCW, O'Colmain BJ, et al. Prevalence of open-angle glaucoma among adults in the United States. *Arch Ophthalmol*.

2004;122(4):532–538, doi:10.1001/archopht.122.4.532.

3. Kwon YH, Fingert JH, Kuehn MH, Alward WLM. Primary open-angle glaucoma. *N Engl J Med*. 2009;360(11):1113–1124, doi:10.1056/NEJMra0804630.
4. Weinreb RN, Khaw PT. Primary open-angle glaucoma. *Lancet*. 2004;363(9422):1711–1720, doi:10.1016/S0140-6736(04)16257-0.
5. Iyer JV, Boland MV, Jefferys J, Quigley H. Defining glaucomatous optic neuropathy using objective criteria from structural and functional testing. *Br J Ophthalmol*. 2021;105(6):789–793, doi:10.1136/bjophthalmol-2020-316237.
6. Huang D, Swanson EA, Lin CP, et al. Optical coherence tomography. *Science*. 1991;254(5035):1178–1181.
7. Mansouri K, Leite MT, Medeiros FA, Leung CK, Weinreb RN. Assessment of rates of structural change in glaucoma using imaging technologies. *Eye*. 2011;25(3):269–277, doi:10.1038/eye.2010.202.
8. Sung KR, Wollstein G, Kim NR, et al. Macular assessment using optical coherence tomography for glaucoma diagnosis. *Br J Ophthalmol*. 2012;96(12):1452–1455, doi:10.1136/bjophthalmol-2012-301845.
9. Sung KR, Kim JS, Wollstein G, Folio L, Kook MS, Schuman JS. Imaging of the retinal nerve fibre layer with spectral domain optical coherence tomography for glaucoma diagnosis. *Br J Ophthalmol*. 2011;95(7):909–914, doi:10.1136/bjo.2010.186924.
10. Tan O, Chopra V, Lu ATH, et al. Detection of macular ganglion cell loss in glaucoma by Fourier-domain optical coherence tomography. *Ophthalmology*. 2009;116(12):2305–2314.e2. doi:10.1016/j.ophtha.2009.05.025.
11. Silverman AL, Hammel N, Khachatryan N, et al. Diagnostic accuracy of the Spectralis and cirrus reference databases in differentiating between healthy and early glaucoma eyes. *Ophthalmology*. 2016;123(2):408–414, doi:10.1016/j.ophtha.2015.09.047.
12. Huang XR, Knighton RW, Cavuoto LN. Microtubule contribution to the reflectance of the retinal nerve fiber layer. *Invest Ophthalmol Vis Sci*. 2006;47(12):5363–5367, doi:10.1167/iovs.06-0451.
13. Huang XR, Zhou Y, Knighton RW, Kong W, Feuer WJ. Wavelength-dependent change of retinal nerve fiber layer reflectance in glaucomatous retinas. *Invest Ophthalmol Vis Sci*. 2012;53(9):5869–5876, doi:10.1167/iovs.12-10001.
14. Huang XR, Zhou Y, Kong W, Knighton RW. Reflectance decreases before thickness changes in the retinal nerve fiber layer in glaucomatous retinas. *Invest Ophthalmol Vis Sci*. 2011;52(9):6737–6742, doi:10.1167/iovs.11-7665.
15. Yi J, Chen S, Shu X, Fawzi AA, Zhang HF. Human retinal imaging using visible-light optical coherence tomography guided by scanning laser ophthalmoscopy. *Biomed Opt Express BOE*. 2015;6(10):3701–3713, doi:10.1364/BOE.6.003701.
16. Chong SP, Bernucci M, Radhakrishnan H, Srinivasan VJ. Structural and functional human retinal imaging with a fiber-based visible light OCT ophthalmoscope. *Biomed Opt Express*. 2016;8(1):323–337, doi:10.1364/BOE.8.000323.
17. Shu X, Beckmann LJ, Zhang HF. Visible-light optical coherence tomography: a review. *J Biomed Opt*. 2017;22(12):121707, doi:10.1117/1.JBO.22.12.121707.
18. Song W, Zhou L, Zhang S, Ness S, Desai M, Yi J. Fiber-based visible and near infrared optical coherence tomography (vnOCT) enables quantitative elastic light scattering spectroscopy in human retina. *Biomed Opt Express BOE*. 2018;9(7):3464–3480, doi:10.1364/BOE.9.003464.
19. Song W, Zhang L, Ness S, Yi J. Wavelength-dependent optical properties of melanosomes in retinal pigmented epithelium and their changes with melanin bleaching: a numerical study. *Biomed Opt Express BOE*. 2017;8(9):3966–3980, doi:10.1364/BOE.8.003966.
20. Zhang T, Kho AM, Zawadzki RJ, et al. Visible light OCT improves imaging through a highly scattering retinal pigment epithelial wall. *Opt Lett OL*. 2020;45(21):5945–5948, doi:10.1364/OL.405398.
21. Zhang X, Hu J, Knighton RW, Huang XR, Puliafito CA, Jiao S. Dual-band spectral-domain optical coherence tomography for in vivo imaging the spectral contrasts of the retinal nerve fiber layer. *Opt Express OE*. 2011;19(20):19653–19659, doi:10.1364/OE.19.019653.
22. Yi J, Radosevich AJ, Rogers JD, et al. Can OCT be sensitive to nanoscale structural alterations in biological tissue? *Opt Express*. 2013;21(7):9043–9059, doi:10.1364/OE.21.009043.
23. Lal C, Alexandrov S, Rani S, Zhou Y, Ritter T, Leahy M. Nanosensitive optical coherence tomography to assess wound healing within the cornea. *Biomed Opt Express BOE*. 2020;11(7):3407–3422, doi:10.1364/BOE.389342.
24. Song W, Fu S, Song S, et al. Longitudinal detection of retinal alterations by visible and

near-infrared optical coherence tomography in a dexamethasone-induced ocular hypertension mouse model. *Neurophotonics*. 2019;6(4):041103, doi:10.1117/1.NPh.6.4.041103.
25. Chylack LT, Leske MC, McCarthy D, Khu P, Kashiwagi T, Sperduto R. Lens opacities classification system II (LOCS II). *Arch Ophthalmol*. 1989;107(7):991–997, doi:10.1001/archopht.1989.01070020053028.
26. Song W, Shao W, Yi W, et al. Visible light optical coherence tomography angiography (vis-OCTA) facilitates local microvascular oximetry in the human retina. *Biomed Opt Express BOE*. 2020;11(7):4037–4051, doi:10.1364/BOE.395843.
27. Knighton RW, Huang XR. Directional and spectral reflectance of the rat retinal nerve fiber layer. *Invest Ophthalmol Vis Sci*. 1999;40(3):639–647.
28. Radosevich AJ, Yi J, Rogers JD, Backman V. Structural length-scale sensitivities of reflectance measurements in continuous random media under the Born approximation. *Opt Lett OL*. 2012;37(24):5220–5222, doi:10.1364/OL.37.005220.
29. Itzkan I, Qiu L, Fang H, et al. Confocal light absorption and scattering spectroscopic microscopy monitors organelles in live cells with no exogenous labels. *Proc Natl Acad Sci U S A*. 2007;104(44):17255–17260, doi:10.1073/pnas.0708669104.
30. Liu S, Wang B, Yin B, et al. Retinal nerve fiber layer reflectance for early glaucoma diagnosis. *J Glaucoma*. 2014;23(1):e45, doi:10.1097/IJG.0b013e31829ea2a7.
31. Gardiner SK, Demirel S, Reynaud J, Fortune B. Changes in retinal nerve fiber layer reflectance intensity as a predictor of functional progression in glaucoma. *Invest Ophthalmol Vis Sci*. 2016;57(3):1221–1227, doi:10.1167/iovs.15-18788.
32. Mwanza JC, Budenz DL, Warren JL, et al. Retinal nerve fibre layer thickness floor and corresponding functional loss in glaucoma. *Br J Ophthalmol*. 2015;99(6):732–737, doi:10.1136/bjophthalmol-2014-305745.
33. Bowd C, Zangwill LM, Weinreb RN, Medeiros FA, Belghith A. Estimating optical coherence tomography structural measurement floors to improve detection of progression in advanced glaucoma. *Am J Ophthalmol*. 2017;175:37–44, doi:10.1016/j.ajo.2016.11.010.
34. Zhang T, Kho AM, Srinivasan VJ. Improving visible light OCT of the human retina with rapid spectral shaping and axial tracking. *Biomed Opt Express BOE*. 2019;10(6):2918–2931, doi:10.1364/BOE.10.002918.
35. Pi S, Hormel TT, Wei X, Cepurna W, Morrison JC, Jia Y. Imaging retinal structures at cellular-level resolution by visible-light optical coherence tomography. *Opt Lett OL*. 2020;45(7):2107–2110, doi:10.1364/OL.386454.
36. Chen S, Shu X, Nesper PL, Liu W, Fawzi AA, Zhang HF. Retinal oximetry in humans using visible-light optical coherence tomography [Invited]. *Biomed Opt Express BOE*. 2017;8(3):1415–1429, doi:10.1364/BOE.8.001415.
37. Pi S, Hormel TT, Wei X, et al. Retinal capillary oximetry with visible light optical coherence tomography. *Proc Natl Acad Sci U S A*. 2020;117(21):11658–11666, doi:10.1073/pnas.1918546117.
38. Yi J, Wei Q, Liu W, Backman V, Zhang HF. Visible-light optical coherence tomography for retinal oximetry. *Opt Lett OL*. 2013;38(11):1796–1798, doi:10.1364/OL.38.001796.